INSTITUTE OF PHYSICS PUBLISHING PHYSICS IN MEDICINE AND BIOLOGY

Phys. Med. Biol. **47** (2002) 2961–2972 PII: S0031-9155(02)34244-1

Measurements of MTF and SNR(f) using a subtraction method in MRI

Tosiaki Miyati[1], Hiroshi Fujita[2], Toshio Kasuga[1], Kichiro Koshida[1], Shigeru Sanada[1], Tatsuo Banno[3], Mitsuhito Mase[4] and Kazuo Yamada[4]

[1] Department of Radiological Technology, School of Health Sciences, Faculty of Medicine, Kanazawa University, 5-11-80, Kodatsuno, Kanazawa, Ishikawa 920-0942, Japan
[2] Department of Information Science, Faculty of Engineering, Gifu University, Yanagido 1-1, Gifu 501-1193, Japan
[3] Department of Central Radiology, Nagoya City University Hospital, 1 Kawasumi, Mizuho-cho, Mizuho-ku, Nagoya, Aichi 467-8602, Japan
[4] Department of Neurosurgery, Nagoya City University Medical School, 1 Kawasumi, Mizuho-cho, Mizuho-ku, Nagoya, Aichi 467-8602, Japan

E-mail: ramiyati@mhs.mp.kanazawa-u.ac.jp

Received 26 February 2002, in final form 20 May 2002
Published 1 August 2002
Online at stacks.iop.org/PMB/47/2961

Abstract

A method was developed for accurate measurement of the modulation transfer function (MTF) and signal-to-noise ratio in the spatial frequency domain (SNR(f)) of magnetic resonance images (MRI). The MTF was calculated from the complex images of a line object which were obtained by the subtraction of two separately acquired data sets of a specially designed phantom with a sliding sheet. Moreover, the SNR(f) was calculated from the MTF and Wiener spectrum, both of which were determined using the same phantom configuration. The MTFs and SNR(f)s in the conventional spin-echo (SE) and turbo SE, in which the effective echo time was set to the first echo, were evaluated by changing the T2 of the phantom and the echo train length. The MTFs in the positive and negative frequencies indicated the effect of the k-space trajectory for each pulse sequence. SNR(f)s gave spatial frequency information that was not obtained with conventional methods. In this method, the influence of image nonuniformity and unwanted artefacts (edge and ghost) could be eliminated. An analysis of the MTF and the SNR in the spatial frequency domain provides additional information for the assessment of image quality in MRI.

1. Introduction

The spatial resolution and signal-to-noise ratio (SNR) are key indicators (EEC Concerted Research Project 1988, National Electrical Manufacturers Association 1988, 1991,

Price *et al* 1990, Och *et al* 1992, Lerski and de Certaines 1993, Internal Commission on Radiation Units and Measurements 1996) in the evaluation of the quality of magnetic resonance images (MRI). In addition to quality control, they are also important in assessing the effect of alterations to MRI systems, or in comparing the pulse sequences.

There are a number of reports on methods to assess resolution properties (Sones and Barnes 1984, Lerski *et al* 1987, 1988, EEC Concerted Research Project 1988, Mohapatra *et al* 1991, Steckner *et al* 1992, 1993, 1994, Lerski and de Certaines 1993, Pipe and Duerk 1995, Internal Commission on Radiation Units and Measurements 1996, McRobbie 1997, Bourel *et al* 1999, Fain *et al* 1999) in MRI. Visual evaluation with bar patterns (Price *et al* 1990) or hole phantoms, and the development of pulse sequences to produce a point spread function (PSF) directly (Robson *et al* 1997), have also been reported. Visual evaluation lacks objectivity, and pulse sequences producing a PSF cannot be readily created with commercial imaging equipment. Ideally, resolution properties in MRI should be quantified by the modulation transfer function (MTF) (Price *et al* 1990, Lerski and de Certaines 1993). Steckner *et al* (1992, 1993, 1994) pointed out various problems in MTF measurements of MRI; for example, any nonconstant phase response can cause errors in MTF measurements obtained from magnitude images. To deal with these problems, they established a method for measuring the MTFs in positive and negative spatial frequencies from a complex edge spread function (ESF) (Steckner *et al* 1994). However, with their method, measurements and processing are difficult and highly complex (Internal Commission on Radiation Units and Measurements 1996). Thus, we have developed a convenient new method to measure the MTF of MRI by using the subtraction of two separately acquired data sets of a specially designed sliding sheet phantom. We were able to obtain the MTFs in positive and negative spatial frequencies from the line spread functions (LSFs) of complex images of a line object.

In addition to the MTF measurement, we determined the Wiener spectra for nonstructured (random) noise (National Electrical Manufacturers Association 1988, Price *et al* 1990, Kaufman *et al* 1989, Sijbers *et al* 1996) by using the same phantom configuration as for the MTF, and then calculated SNRs (Internal Commission on Radiation Units and Measurements 1996) for positive and negative spatial frequencies (SNR(f)s), because the SNR is not necessarily independent of spatial frequency. For example, because fast sequences such as the rapid acquisition relaxation enhanced (RARE) (Hennig *et al* 1986) sequence affect the MTF (Farzaneh *et al* 1990, Holsinger and Riederer 1990, Mulkern *et al* 1990, 1991, Constable *et al* 1992, Listerud *et al* 1992, Norris *et al* 1992, Constable and Gore 1992, Vlaardingerbroek and den Boer 1996, Melhem *et al* 1996, Kholmovski *et al* 2000), the SNR will be dependent upon spatial frequency.

There are no reports that both MTFs and SNR(f)s were actually measured and evaluated using the same phantom. The present report describes a 'subtraction method' for analysing the MTF and SNR(f) using a process of subtraction of the complex images, and demonstrates the results of the RARE sequences in which the effective TE is set at the first echo.

2. Materials and methods

2.1. Phantom

As shown in figures 1(a)–(d), the phantom is structured so that a 70-mm-wide thin sliding polyethylene terephthalate (PET) sheet can be moved in and out of the image slice along a 50-mm-high Plexiglas guiding frame in a hemispheric Plexiglas container with an inner diameter of 170 mm. The thickness of the PET sheet was set at 400 μm, which was determined by increasing the thickness of the sheet (from 100 μm at intervals of 100 μm) until the SNR

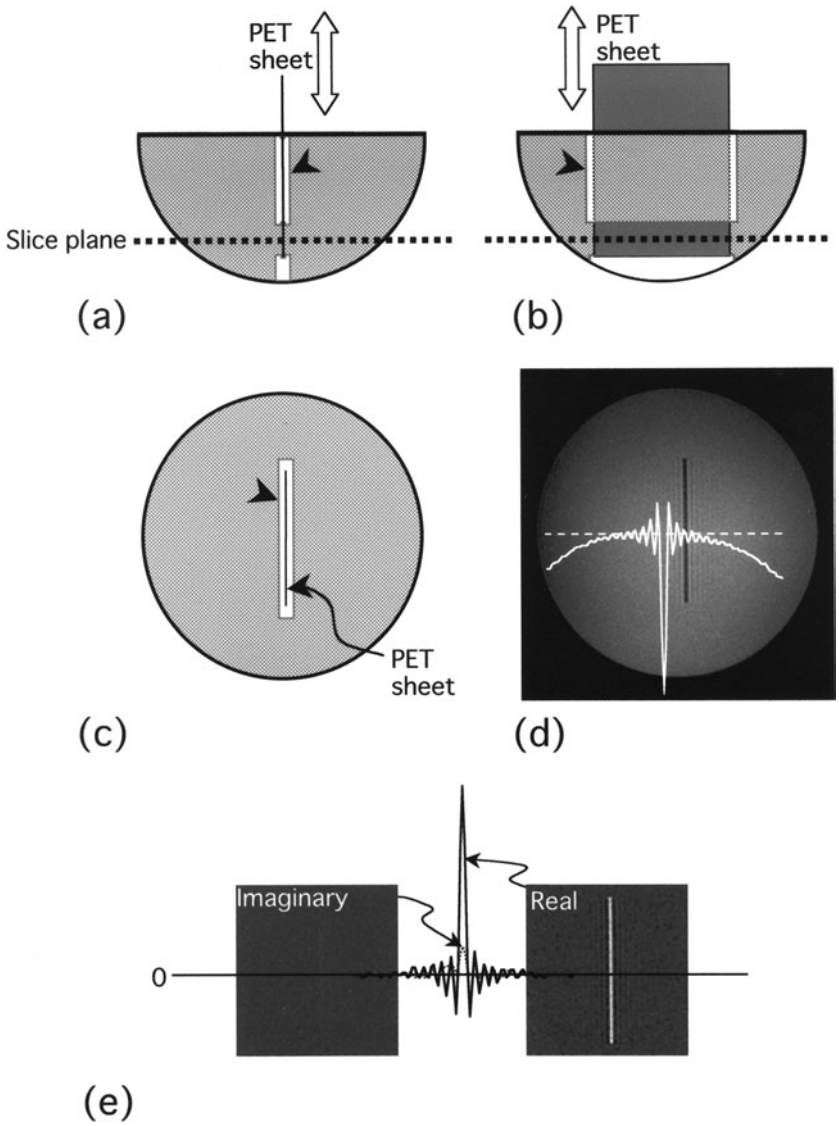

Figure 1. ((a) and (b)) Orthogonal side views and (c) top view of the hemispherical phantom used for the subtraction method. A thin sliding PET sheet ((a), (b) and curved arrow in (c)) can be moved in and out of the image slice (horizontal dotted lines in (a) and (b)) along the guiding frame. (d) The phantom image (real part) and the signal intensity profile of the line object of the first scan. (e) Subtracted complex images (real part (right), imaginary part (left)) and the profiles.

value of the integral LSF (= ESF) of the conventional spin-echo (SE) (see section 2.4) reached the same level as Stekner *et al* (1994) reported (SNR of the ESF phantom image = 210:1) . The SNR of the integral LSF was calculated by dividing the plateau value of the integral LSF by the standard deviation of the uniform phantom region in a subtracted magnitude image. If the PET sheet is too thin, the SNR becomes extremely low. However, because the MTF decreases at a high frequency along with the increase in the thickness of the PET sheet, correction of the thickness is required (for details, see section 2.2).

A solution, selected for its suitability for the study, is sealed inside the container. The solution does not leak out because the PET sheet fits the guiding frame with fluorine grease which is not mixed with the solution. Thus, it is possible to obtain measurements at various slice orientations. In this study, we prepared long T2 and short T2 phantoms to investigate the effects of T2 in the RARE sequences on the MTF and SNR. The long T2 phantom was filled with copper sulfate solution ($CuSO_4{\cdot}5H_2O$: 0.77 g/l), which gave a T1 of 423 ms and a T2 of 365 ms at 1.5 T, whereas the short T2 phantom was filled with manganese chloride solution ($MnCl_2{\cdot}4H_2O$: 0.05 g/l), which gave a T1 of 481 ms and a T2 of 52 ms at 1.5 T. These relaxation times of the solutions were determined with a multi-echo SE sequence interleaved with a multi-echo inversion recovery sequence (In den Kleef and Cuppen 1987).

2.2. MTF measurement and analysis

The MTF is carried out separately for the phase-encoding and frequency-encoding directions. The phantom is first placed in the relevant radio-frequency coil, and it is essential that the phantom is held completely still. At this time, a space of about 3 cm is ensured so that the PET sheet can be withdrawn. As shown in figures 1(a) and (b), the slice plane is positioned exactly perpendicular to the PET sheet and does not intersect the guiding frame. The line object is accurately aligned with the coordinate system of the imaging plane. In MRI, the MTF can be an unaliased MTF (Steckner *et al* 1993, 1994) because the raw data are acquired in the Fourier domain (Kholmovski *et al* 2000, Riederer 1993). Thus, the angulated slit method (Fujita *et al* 1989, 1992) is not needed.

Initially, a first scan is done, and real and imaginary images are obtained (complex images A). Because the edge of the hemispherical phantom is blurred by the partial volume effect, the ringing artefact due to the phantom edge is reduced. The field of view (FOV) should be larger than the cross-sectional area to eliminate the aliasing artefact, and the raw data echo peak should be centred in the data acquisition window (Steckner *et al* 1994). As shown in figure 1(d), the baseline of the LSF profile is distorted, causing low-frequency modulation, because the image uniformity of MRI systems is generally not so high (Lerski and de Certaines 1993). Immediately after the first scan, the PET sheet is withdrawn about 2 cm so that the PET sheet and slice plane do not intersect. In order to minimize the effect of fluid motion, after 2 min, the second scan is made (complex images B) with exactly the same scan parameters as for complex images A. Complex images A are subtracted from complex images B so that a uniform LSF profile is obtained, and ringing artefacts induced by the edge of the hemispherical phantom and ghost artefacts are almost eliminated (figure 1(e)).

Next, more than 100 complex LSFs with sufficient length (in this experiment, 128 pixels) obtained from the subtraction image are averaged (Steckner *et al* 1994), and the SNR of the LSF becomes higher. After a Fourier transform is conducted on the complex LSF data, the following calculation is needed to correct the thickness of the PET sheet. Uncorrected LSF ($\mathrm{LSF}'(x)$) and MTF ($\mathrm{MTF}'(f)$) are expressed as equations (1) and (2):

$$\mathrm{LSF}'(x) = \mathrm{LSF}(x) * \mathrm{rect}(x) \tag{1}$$

$$\mathrm{MTF}'(f) = F(\mathrm{LSF}(x))F(\mathrm{rect}(x)) = \mathrm{MTF}(f)\sin(\pi f d)/\pi f d, \tag{2}$$

where $\mathrm{LSF}(x)$ and $\mathrm{MTF}(f)$ denote the correct LSF and correct MTF, $*$ is convolution, $\mathrm{rect}(x)$ is the rectangle function due to the thickness (d) of the PET sheet, f is the spatial frequency and F represents the Fourier transform operator. Therefore, the correct MTF in positive and negative spatial frequencies is calculated with the following equation:

$$\mathrm{MTF}(f) = \mathrm{MTF}'(f)\pi f d/\sin(\pi f d). \tag{3}$$

2.3. SNR(f) measurement and analysis

We first determined the Wiener spectra. The subtraction method is intended to measure thermal and other broadband, nonstructured noise, and specifically does not address low-frequency variations in an image or artefacts as defined herein (National Electrical Manufacturers Association 1988, Price *et al* 1990, Internal Commission on Radiation Units and Measurements 1996, Kaufman *et al* 1989, Sijbers *et al* 1996). Structured noise such as motion or pulsation artefacts is also an important component of diagnostic images. Analysis of structured noise, however, must be conducted by a completely different method; therefore, it is not included in the present study.

The technique we employed to calculate the digital Wiener spectrum is similar to the method established by Giger *et al* (1986). The phantom configuration of the second scan in the MTF measurement described above is left unchanged, and the acquisition parameters are set according to the purpose of the experiment. Two identical scans are run sequentially with less than 5 min intervals between them (complex images C and complex images D). If complex images B are used as a substitute for complex images C, only complex images D are obtained under exactly the same scan parameter as complex images B. To eliminate structured noise and low-frequency variations in the images, noise images are calculated by subtracting complex images C and complex images D. The noise data have a mean value of almost zero because the subtracted images are uniform.

The Wiener spectra were evaluated for 128×128 pixels at the central part of the subtracted noise images. A hypothetical scanning slit (Fujita *et al* 1989, Giger *et al* 1986) with a width of one pixel was made, and the slit length was determined by increasing the length of the slit until the Wiener spectral value reached a plateau (in this experiment, 16 pixels). The slit trace data are averaged with the noise data over a given slit length. The fast Fourier transform method is employed for the spectrum calculations, and the spectrum is multiplied by the slit length. The spectra in positive and negative frequencies obtained from all the slit traces (in this experiment, 16 traces) are averaged, then smoothed by use of a running mean. The Wiener spectra of the original images are obtained by dividing the spectra of the subtracted images by 2 (Giger *et al* 1986). Finally, the SNR(f)s are calculated from the Wiener spectra, the MTFs and mean signal intensities of the original (pre-subtracted) images (S). $\mathrm{SNR}^2(f)$ (Internal Commission on Radiation Units and Measurements 1996) is defined as follows:

$$\mathrm{SNR}^2(f) = S^2\,\mathrm{MTF}^2(f)/WS(f). \tag{4}$$

2.4. Experimental conditions

All scans were performed using the above-mentioned phantom with a loading device in the head coil on a 1.5 T MR system (Gyroscan ACS II, Philips Medical Systems International, Best, The Netherlands). Data were collected by the use of a conventional SE and RARE sequence (turbo SE) with the effective TE set to the first echo (Vlaardingerbroek and den Boer 1996, Melhem *et al* 1996) (figure 2). Echo train length (ETL) was changed to 1 (=conventional SE), 3, 7 and 15, and the effects of T2 relaxation (52 ms and 365 ms) were investigated for frequency and phase-encoding direction. When the ETL was 1, 3, 7 and 15, the number of phase encoded lines was 256 (256 segments), 255 (85 segments), 252 (36 segments) and 255 (17 segments), respectively. Therefore, the turbo SE acquisition time was about 1/ETL that of the conventional SE. All sequences were used with parameters of 1500/11 ms (TR/TE), 256 frequency-encoded points, 11 ms echo spacing, 3 mm slice thickness, 256×256 mm FOV and 4 signals averaged. The raw data matrix was zero padded to 512×512 to extend the spatial frequency axis and examine the cut-off frequency

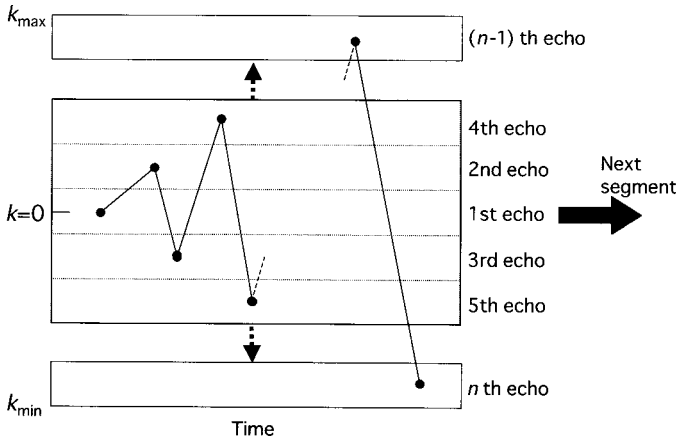

Figure 2. Profile order of turbo SE which set effective TE at the first echo. The profiles are numbered according to the order of the k values in the phase-encode direction. The profile numbers are taken to be 0, $+S$, $-S$, $+2S$, $-2S$, $3S$, $-3S$, ..., $nS/2$ and $-nS/2$ for the first segment and followed by similar segments, but then started with another first profile number between $(-S + 1)/2$ and $(S - 1)/2$, until all profiles were sampled. S is the number of segments and n is ETL.

region of the MTF, and no filter such as a Hanning window was applied to the raw data. Shimming with linear gradient components was performed in all the imaging studies.

3. Results and discussion

3.1. MTF

Figure 3 shows the MTFs measured using the subtraction method. The MTF measurements with conventional SE correspond well with the results of Steckner *et al* (1994) (open circles in figures 3(a)–(d)). The MTF values fell dramatically at the theoretically predicted cut-off frequency in both the frequency-encode and phase-encode directions, and the MTF in the positive frequency had the same shape as that in the negative frequency. MTFs of the turbo SE in the frequency-encode direction, similar to the conventional SE MTFs, dropped sharply at the cut-off frequency in the form of a rectangular function (figures 3(a) and (c)).

On the other hand, MTFs of the turbo SE in the phase-encode direction declined at high spatial frequencies with increases in ETL. The shorter the T2, the greater was the ratio of the decline in MTF (figures 3(b) and (d)). The turbo SE MTFs in the phase-encode direction were not symmetrical at a frequency of 0, and were stepwise because of the dependence on the T2-weighting and discontinuity of each segment of k-space (Vlaardingerbroek and den Boer 1996) (figure 3(b) and (d)). Thus, the MTF calculated from the complex LSFs, which retain image phase information, was not always symmetric for the frequency of 0 (e.g., half Fourier reconstruction algorithm (Steckner *et al* 1994)). Therefore, there are cases in which the two-sided MTF provides more detailed information on MRI resolution properties which cannot be obtained from the magnitude image MTF. It is clear, then, that if the k-space trajectories of the pulse sequence and the T2 relaxation time are known, the MTF can be simulated. However, when confirming the simulation, or when the details of the pulse sequence are unknown, the MTF can be determined by this method.

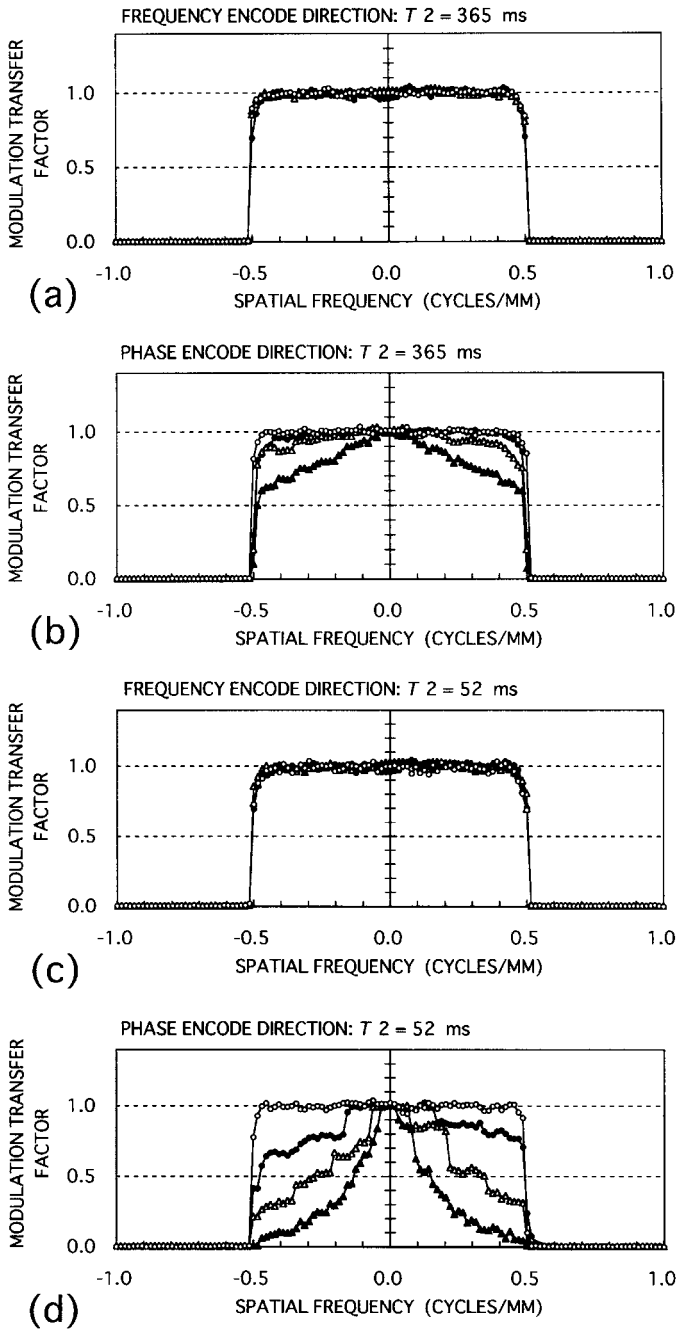

Figure 3. MTFs of conventional SE (-○-) and turbo SE (ETL of 3 (-●-), 7 (-△-) and 15 (-▲-)) measured with the subtraction method at ((a) and (b)) long T2 phantom (365 ms) and ((c) and (d)) short T2 phantom (52 ms) in the frequency- and phase-encoding directions, respectively.

Because the raw data themselves for the Fourier transform MRI reconstruction correspond to the spatial frequency (Kholmovski *et al* 2000, Riederer 1993), it may be possible to

analyse the MTF directly from the raw data. However, it is difficult to extract raw data on all commercial MRI imagers, and to obtain a sufficient SNR to calculate the MTF. Therefore, averaging a number of LSFs in the image domain and combining the subtraction and deconvolution processes to raise the SNR is a convenient and reliable method. Actually, the SNR of the LSF with this method was at the same level as the edge method (Steckner *et al* 1994). The plateau values of the rectangular MTF for the conventional SE were within the coefficient of variation of 2%. Although the edge method MTF has the highest SNR at low spatial frequencies (Cunningham and Reid 1992), in MRI the edge method is difficult (Internal Commission on Radiation Units and Measurements 1996) and requires some corrections and processing (Steckner *et al* 1994). With this subtraction method, the effects of image nonuniformity (Lerski and de Certaines 1993) could be easily corrected, and the LSF could be obtained directly without calculating from the ESF and without a correction of the discrete derivative (Steckner *et al* 1994). Furthermore, Gibb's ringing artefact (Steckner *et al* 1994) induced by an unwanted edge of the hemispherical phantom could be removed, because the edge was blurred by a partial volume effect, and the subtraction process was performed in sequential images. At the same time, the effects of unnecessary artefacts such as a ghost could also be eliminated. However, when some systematic variations cannot be removed in the subtracted images because the scanner does not remain completely stable between acquisitions (National Electrical Manufacturers Association 1988, Magnusson and Olsson 2000), one must use an alternate method with magnitude subtraction images and apply a polynomial fitting process (Giger *et al* 1986). The MTF calculated from the magnitude subtraction images does not produce the distortions due to the nonlinear problem, but two-sided MTFs cannot be obtained because the phase information in the image domain is removed by the magnitude operator (Steckner *et al* 1994).

3.2. SNR(f)

Figure 4 shows the Wiener spectra measured with the subtraction method for computing the SNR(f). With both the conventional and turbo SE, the Wiener spectra in the frequency-encode and phase-encode directions were constant up to the cut-off frequencies, and then dropped rapidly beyond the cut-off frequency. These results indicate that, without some kind of spatial frequency filter, the Wiener spectrum is independent of spatial frequency until the cut-off frequency. The Wiener spectrum could be measured with the same phantom configuration as for MTF measurements, so that the SNR(f) could be easily and accurately obtained, as shown in figure 5. In both the frequency-encode and phase-encode directions, the SNR^2(f)s of the conventional SE had the same shape and dropped sharply at the cut-off frequency (open circles in figures 5(a)–(d)) because the MTFs and the Wiener spectra were cut off above the Nyquist frequency due to the finite sampling effect. The SNR^2(f)s of the turbo SE in the frequency-encode direction also gave the same results as conventional SE (figures 5(a) and (c)). In the frequency-encode direction, the SNR^2(f)s showed an average difference of 32% between the long T2 and short T2 phantoms (figures 5(a) and (c)). This was due to differences in the respective T2 and T1 of the phantoms, because the coil loading of each solution was nearly the same. This difference corresponded with the theoretical value (33%) calculated with the relaxation times of each solution.

In the phase-encode direction, the SNR^2(f)s of the turbo SE decreased with increases in ETL. The shorter the T2, the greater was the ratio of the decline in SNR^2 (figures 5(b) and (d)). However, SNRs without spatial frequency information of the conventional SE and all turbo SE measured with the standard test method (National Electrical Manufacturers Association 1988, Price *et al* 1990) were nearly the same for each of the phantoms; the turbo SE acquisition time

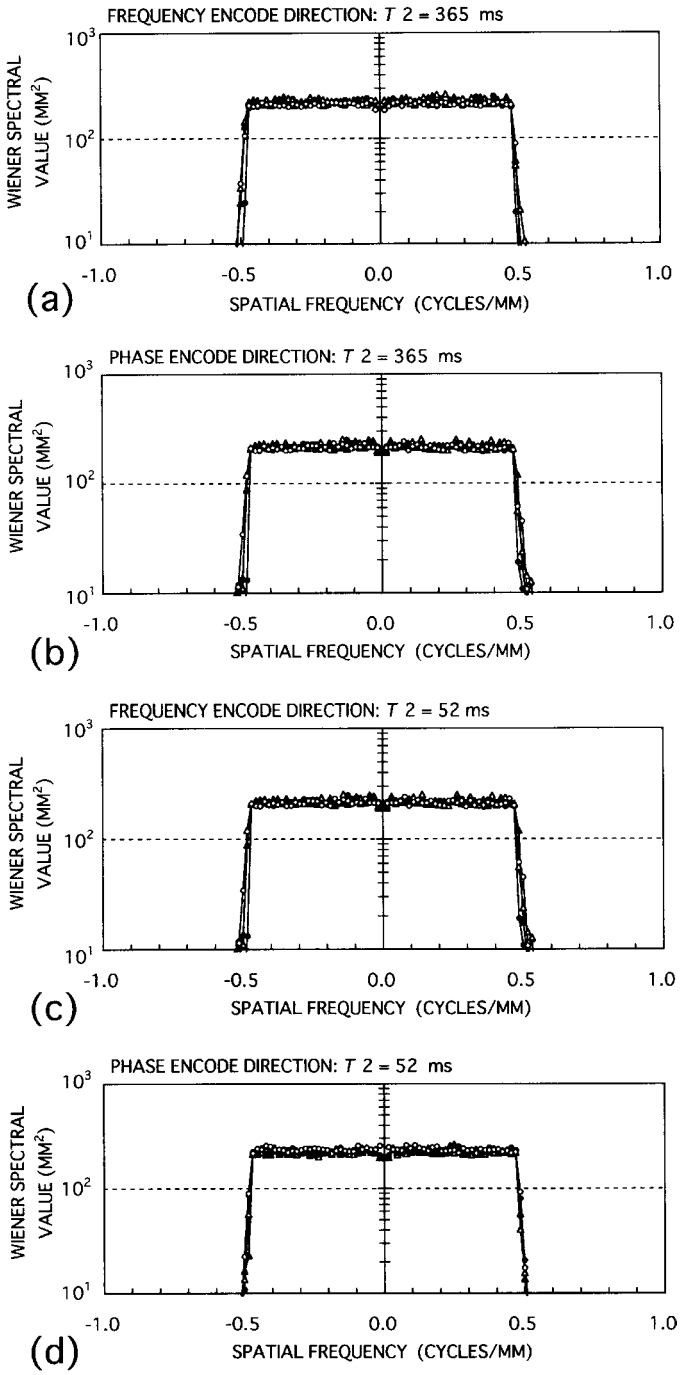

Figure 4. Wiener spectra of conventional SE (-○-) and turbo SE (ETL of 3 (-●-), 7 (-△-) and 15 (-●-)) measured with the subtraction method at ((a) and (b)) long T2 phantom (365 ms) and ((c) and (d)) short T2 phantom (52 ms) in the frequency- and phase-encoding directions, respectively.

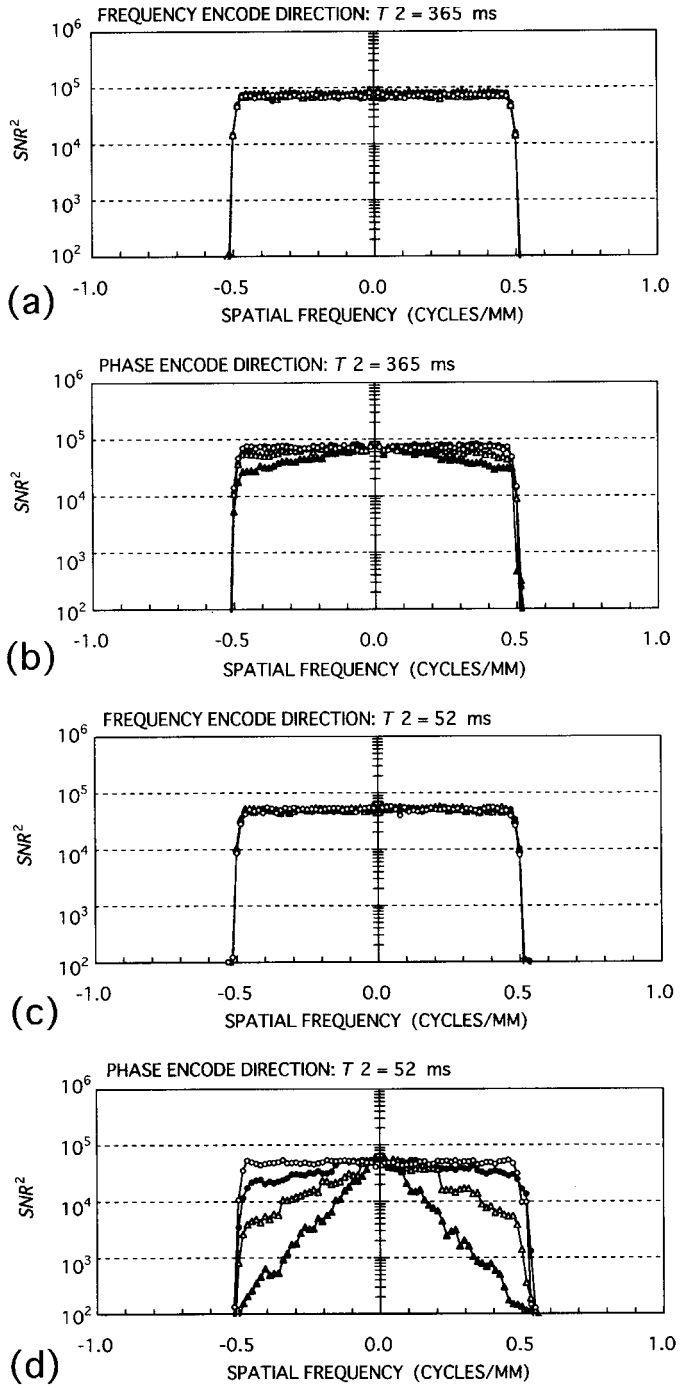

Figure 5. $SNR^2(f)$ of conventional SE (-○-) and turbo SE (ETL of 3 (-●-), 7 (-△-) and 15 (-▲-)) measured with the subtraction method at ((a) and (b)) long T2 phantom (365 ms) and ((c) and (d)) short T2 phantom (52 ms) in the frequency- and phase-encoding directions, respectively.

was about 1/ETL that of the conventional SE. Thus, in evaluations of fast pulse sequences such as RARE SE, there are times when evaluation of SNR that does not have frequency information is insufficient, and evaluation of the SNR in the spatial frequency is more useful. Moreover, as in the $SNR^2(f)$ of the turbo SE in the phase-encode direction (figures **5**(b) and (d)), the $SNR^2(f)$ did not have perfect symmetry in the positive and negative frequencies, indicating the need for evaluations of both frequencies.

4. Conclusion

We have developed a 'subtraction method' with which the MTF and SNR in the positive and negative spatial frequencies can be evaluated easily under the same phantom configuration. With this method, the influence of image nonuniformity and unwanted artefacts could be eliminated. The analysis of the MTF and SNR in the spatial frequency domain by use of the subtraction method provides additional information for MR image quality assessment and may be useful for the evaluation of pulse sequences.

References

Bourel P, Gibon D, Coste E, Daanen V and Rousseau J 1999 Automatic quality assessment protocol for MRI equipment *Med. Phys.* **26** 2693–700

Constable R T, Anderson A W, Zhong J and Gore J C 1992 Factors influencing contrast in fast spin-echo MR imaging *Magn. Reson. Imaging* **10** 497–511

Constable R T and Gore J C 1992 The loss of small objects in variable TE imaging: implications for FSE, RARE, and EPI *Magn. Reson. Med.* **28** 9–24

Cunningham I A and Reid B K 1992 Signal and noise in modulation transfer function determinations using the slit, wire, and edge techniques *Med. Phys.* **19** 1037–44

EEC Concerted Research Project 1988 Identification and characterization of biological tissues by NMR. Concerted Research Project of the European Economic Community: IV. Protocols and test objects for the assessment of MRI equipment *Magn. Reson. Imaging* **6** 195–9

Fain S B, Riederer S J, Bernstein M A and Huston J III 1999 Theoretical limits of spatial resolution in elliptical-centric contrast-enhanced 3D-MRA *Magn. Reson. Med.* **42** 1106–16

Farzaneh F, Riederer S J and Pelc N J 1990 Analysis of T2 limitations and off-resonance effects on spatial resolution and artifacts in echo-planar imaging *Magn. Reson. Med.* **14** 123–39

Fujita H, Tsai D Y, Itho T, Doi K, Morishita J, Ueda K and Ohtsuka A 1992 A simple method for determining the modulation transfer function in digital radiography *IEEE Trans. Med. Imaging* **11** 34–9

Fujita H, Ueda K, Morishita J, Fujikawa T, Ohtsuka A and Sai T 1989 Basic imaging properties of a computed radiographic system with photostimulable phosphors *Med. Phys.* **16** 52–9

Giger M L, Doi K and Fujita H 1986 Investigation of basic imaging properties in digital radiography: 7. Noise Wiener spectra of II-TV digital imaging systems *Med. Phys.* **3** 131–8

Hennig J, Nauerth A and Friedburg H 1986 RARE imaging: a fast imaging method for clinical MR *Magn. Reson. Med.* **3** 823–33

Holsinger A E and Riederer S J 1990 The importance of phase-encoding order in ultra-short TR snapshot MR imaging *Magn. Reson. Med.* **16** 481–8

In den Kleef J J and Cuppen J J 1987 RLSQ: T1, T2, and rho calculations, combining ratios and least squares *Magn. Reson. Med.* **5** 513–24

Internal Commission on Radiation Units and Measurements 1996 Medical imaging—the assessment of image quality *ICRU Report* 54

Kaufman L, Kramer D M, Crooks L E and Ortendahl D A 1989 Measuring signal-to-noise ratios in MR imaging *Radiology* **173** 265–7

Kholmovski E G, Parker D L and Alexander A L 2000 A generalized k-sampling scheme for 3D fast spin echo *J. Magn. Reson. Imaging* **11** 549–58

Lerski R A and de Certaines J D 1993 Performance assessment and quality control in MRI by Eurospin test objects and protocols *Magn. Reson. Imaging* **11** 817–33

Lerski R A, McRobbie D W, Fitzpatrick M L, Howarth A and Williams J L 1987 Modulation transfer function measurements in magnetic resonance imaging *SMRM Conf.* vol 6, pp 918

Lerski R A, McRobbie D W, Straughan K, Walker P M, de Certaines J D and Bernard A M 1988 Multi-center trial with protocols and prototype test objects for the assessment of MRI equipment. EEC Concerted Research Project *Magn. Reson. Imaging* **6** 201–14

Listerud J, Einstein S, Outwater E and Kressel Y 1992 First principle of fast spin echo *Magn. Reson. Q.* **8** 199–244

Magnusson P and Olsson L E 2000 Image analysis methods for assessing levels of image plane nonuniformity and stochastic noise in a magnetic resonance image of a homogeneous phantom *Med. Phys.* **27** 1980–94

McRobbie D W 1997 A three-dimensional volumetric test object for geometry evaluation in magnetic resonance imaging *Med. Phys.* **24** 737–42

Melhem E R, Jara H and Yucel E K 1996 Multislice T1-weighted hybrid RARE in CNS imaging: assessment of magnetization transfer effects and artifacts *J. Magn. Reson. Imaging* **6** 903–8

Mohapatra S M, Turley J D, Prince J R, Blechinger J C and Wilson D A 1991 Transfer function measurement and analysis for a magnetic resonance imager *Med. Phys.* **18** 1141–4

Mulkern R V, Melki P S, Jakab P, Higuchi N and Jolesz F A 1991 Phase-encode order and its effect on contrast and artifact in single-shot RARE sequences *Med. Phys.* **18** 1032–7

Mulkern R V, Wong S T, Winalski C and Jolesz F A 1990 Contrast manipulation and artifact assessment of 2D and 3D RARE sequences *Magn. Reson. Imaging* **8** 557–66

National Electrical Manufacturers Association 1988 Determination of signal-noise ratio in diagnostic magnetic resonance images *NEMA Standard Publication* No MS1

National Electrical Manufacturers Association 1991 Characterization of special purpose coils for diagnostic magnetic resonance images *NEMA Standard Publication* No MS6

Norris D G, Bornert P, Reese T and Leibfritz D 1992 On the application of ultra-fast RARE experiments *Magn. Reson. Med.* **27** 142–64

Och J G, Clarke G D, Sobol W T, Rosen C W and Mun S K 1992 Acceptance testing of magnetic resonance imaging systems: report of AAPM nuclear magnetic resonance Task Group No 6 *Med. Phys.* **19** 217–29

Pipe J G and Duerk J L 1995 Analytical resolution and noise characteristics of linearly reconstructed magnetic resonance data with arbitrary k-space sampling *Magn. Reson. Med.* **34** 170–8

Price R R, Axel L, Morgan T, Newman R, Perman W, Schneiders N, Selikson M, Wood M and Thomas S R 1990 Quality assurance methods and phantoms for magnetic resonance imaging: report of AAPM nuclear magnetic resonance Task Group No 1 *Med. Phys.* **17** 287–95

Riederer S J 1993 *The Physics of MRI; 1992 AAPM Summer School Proc.* ed M J Bronskill and P Sprawls (New York: AIP) pp 135–64

Robson M D, Gore J C and Constable R T 1997 Measurement of the point spread function in MRI using constant time imaging *Magn. Reson. Med.* **38** 733–40

Sijbers J, Scheunders P, Bonnet N, Van Dyck D and Raman E 1996 Quantification and improvement of the signal-to-noise ratio in a magnetic resonance image acquisition procedure *Magn. Reson. Imaging* **14** 1157–63

Sones R A and Barnes G T 1984 A method to measure the MTF of digital x-ray systems *Med. Phys.* **11** 166–71

Steckner M C, Drost D J and Prato F S 1992 Comments and Reply: 'transfer function measurements and analysis for a magnetic resonance imager' (Mohapatra *et al* 1991) *Med. Phys.* **19** 511–2

Steckner M C, Drost D J and Prato F S 1993 A cosine modulation artifact in modulation transfer function computations caused by the misregistration of line spread profiles *Med. Phys.* **20** 469–73

Steckner M C, Drost D J and Prato F S 1994 Computing the modulation transfer function of a magnetic resonance imager *Med. Phys.* **21** 483–9

Vlaardingerbroek M T and den Boer J A 1998 *Magnetic Resonace Imaging; Theory and Practice* (Berlin: Springer) pp 115–66